CHEMISTRY OF MATERIALS

Article

pubs.acs.org/cm

Elucidating Structure−Composition−Property Relationships of the β-SiAlON:Eu^{2+} Phosphor

Zhenbin Wang, Weike Ye, Iek-Heng Chu, and Shyue Ping Ong*

Department of NanoEngineering, University of California—San Diego, 9500 Gilman Drive, La Jolla, California 92093-0448, United States

Ⓢ *Supporting Information*

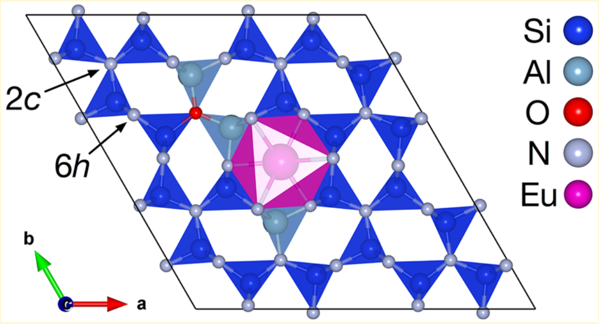

ABSTRACT: In this work, we performed a systematic investigation of structure−composition−property relationships in Eu^{2+}-activated β-SiAlON, one of the most promising narrow-band green phosphors for high-power light-emitting diodes and liquid crystal display backlighting with wide color gamut. Using first-principles calculations, we identified and confirmed various chemical rules for Si−Al, O−N, and Eu activator ordering within the β-SiAlON structure. Through the construction of energetically favorable models based on these chemical rules, we studied the effect of oxygen content and Eu^{2+} activator concentrations on the local EuN_9 activator environment, and its impact on important photoluminescence properties such as emission peak position (using the band gap as a proxy), bandwidth, and thermal quenching resistance. Increasing oxygen content is shown to lead to an increase in Eu−N bond lengths and distortion of the EuN_9 coordination polyhedron, modifying the crystal field environment of the Eu^{2+} activator, and resulting in red-shifting and broadening of the emission. We also show that the calculated excited band structure of β-SiAlON exhibits a large gap between the 5d levels and the conduction band of the host, indicating a large barrier toward thermal ionization (>0.5 eV) and, hence, excellent thermal quenching stability. Based on these insights, we discuss potential strategies for further composition optimization of β-SiAlON.

■ INTRODUCTION

Phosphor-converted light-emitting diodes (pc-LEDs) have emerged as leading candidates for next-generation lighting applications due to their exceptional efficiency and environmental friendliness compared to traditional lighting sources. Among the candidates for green phosphors, β-SiAlON:Eu^{2+} is of particular interest due to its high quantum efficiency, narrow emission bandwidth (full width at half-maximum, or fwhm, of 45−55 nm), and outstanding thermal quenching behavior (90% at 150 °C), which makes it suitable for high-power LEDs as well as liquid crystal display (LCD) backlights with wide color gamut.[1−3]

β-SiAlON is derived from β-Si_3N_4 (Figure 1a) via the substitution of Al and O for Si and N, respectively. Its chemical formula can be formally written as $Si_{6-z}Al_zO_zN_{8-z}$, with z typically ranging from 0 to 4.2.[1−3] The photoluminescence (PL) properties of β-SiAlON can be tuned by modification of z as well as the concentration of the Eu^{2+} activator.[4] Previous experiments[1,3,5] have established that limits on Eu^{2+} doping (<2 mol%) and Al−O substitution concentration ($z < 0.5$) apply for practical applications. Higher z (>1) will not only cause red-shifting of the emission (545−550 nm) with broadened bandwidth (>63 nm) but also result in impurity phase formation and decrease of emission intensity.[1] Hirosaki et al.[5] have previously proposed that a composition of $Eu_{0.00296}Si_{0.41395}Al_{0.01334}O_{0.0044}N_{0.56528}$ (equivalent to $Si_{140}Al_{4.5}O_{1.5}N_{191}$:$Eu^{2+}$ with 0.296 mol% Eu^{2+}, i.e., $z = 0.17$) yields an ideal green emission peak of 535 nm and a narrow bandwidth of 55 nm.

Despite extensive studies, there remains significant ambiguity about the precise structure of β-SiAlON. It has been shown via advanced scanning transmission electron microscopy (STEM) that Eu^{2+} sits at the interstitial site in the large hexagonal channels along the [0001] direction (Figure 1a) because of the large size mismatch between Eu^{2+} and the Si^{4+} and Al^{3+} cations.[6] More recently, Brgoch et al.[7] proposed that the Eu^{2+} ion occupies a distorted 12-fold coordinated environment within these hexagonal channels via extended X-ray adsorption fine structure (EXAFS) measurements. Nevertheless, experimental information about the detailed cation/anion ordering in β-SiAlON:Eu^{2+} remains lacking due to the almost indistinguishable scattering factors of the two substitution pairs, Al^{3+}/Si^{4+} and O^{2-}/N^{3-}, and the low concentration of the Eu^{2+} activator (<2 mol%).[7]

In this work, we elucidate the structure−composition−property relationships in β-SiAlON:Eu^{2+} using density functional theory (DFT) calculations. Using a chemical rule-based screening approach, we identified energetically favorable

Received: August 23, 2016
Revised: November 15, 2016
Published: November 16, 2016

DOI: 10.1021/acs.chemmater.6b03555
Chem. Mater. 2016, 28, 8622−8630

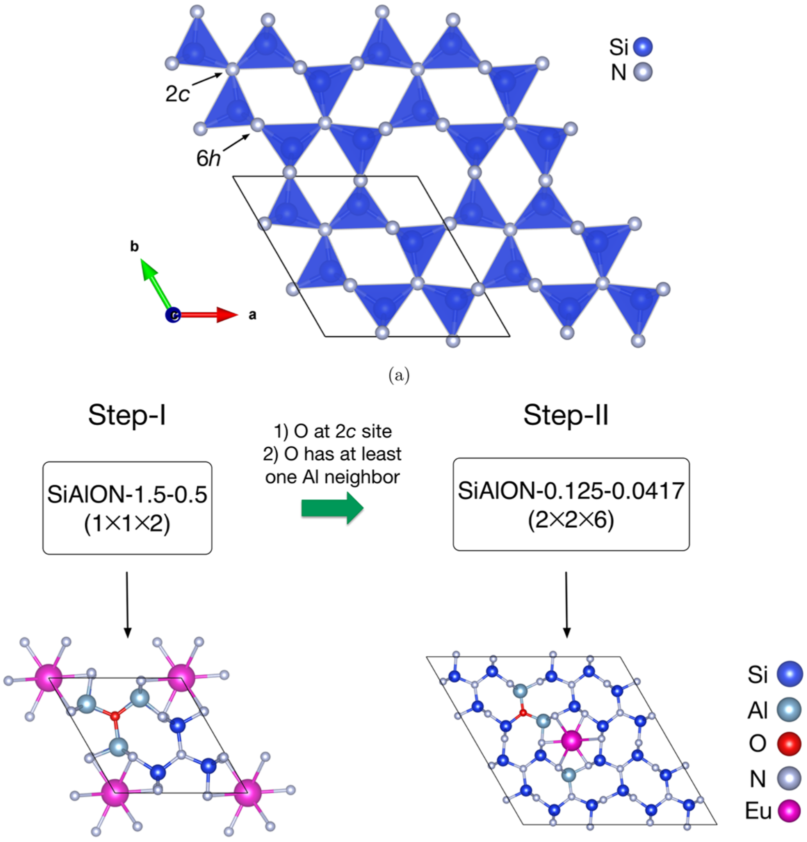

(a)

(b)

Figure 1. (a) Crystal structure of β-Si_3N_4, in which there are two distinct nitrogen sites with Wyckoff symbols 2*c* and 6*h*. The solid line denotes a unit cell. (b) Procedure to identify Al/O/Eu ordering rules in $Si_{6-z}Al_zO_{z-2y}N_{8-z+2y}$:*y*Eu. The crystal structures shown are for the lowest energy structures for the 1×1×2 (left) and 2×2×6 (right) supercells.

structures for β-SiAlON:Eu^{2+} at various z and Eu^{2+} activator concentrations. A systematic study was then carried out on the effect of composition on important PL properties of β-SiAlON:Eu^{2+}, such as the emission peak position, bandwidth, and thermal quenching behavior, using various first-principles descriptors. We successfully predict the red-shifting and broadening of emission with increasing oxygen content. These effects are shown to be the result of a direct causal relationship between composition and local Eu^{2+} activator environment, and its corresponding effect on the Eu^{2+} crystal field. These insights pave the way for not just further composition optimization of β-SiAlON:Eu^{2+}, but potentially other phosphors.

■ METHODS

Density Functional Theory Calculations. All DFT calculations were carried out using Vienna ab initio simulation package (VASP) within the projected-augmented wave method,[8,9] and all crystal structure manipulations and data analysis were performed using Python Materials Genomics (pymatgen) package.[10]

For structure optimizations and energy evaluations, calculations were carried out using the Perdew–Burke–Ernzerhof (PBE) generalized gradient approximation (GGA) functional[11] with the Hubbard U extension (PBE+U)[12] to take into account the strongly localized 4*f* electrons of Eu. An effective Hubbard U of 2.5 eV for the Eu 4*f* orbitals was used, similar to that used by previous work on oxide phosphors.[13] We have shown in our recent work that a similar U value applies for nitride phosphors, and the electronic structure is not highly sensitive to minor changes in U.[14] The energy cutoff was 520 eV. An energy convergence criterion of 5×10^{-5} eV and a k-point mesh of at least 15/Å^{-1} were used to compare the energies of different structure orderings. The low-energy structures identified were subsequently relaxed with more stringent energy and force convergence criteria of 1×10^{-5} eV and 0.01 eV/Å, respectively. Density of states (DOS) calculations were performed with a higher k-point mesh of at least 30/Å^{-1}. The ground state electronic band structure was calculated using similar parameters, but with explicit specification of k-points along high-symmetry directions.[15]

The excited-state band structure of Eu^{2+}-activated β-SiAlON was calculated using constrained DFT where the occupancy of the topmost Eu 4*f* state (at the valence band) was transferred to the lowest 5*d* state (at the conduction band) and kept fixed during the calculations.[13] In these calculations, the crystal structures were first obtained from the excited-state structural optimization under the same occupancy distribution.

To obtain more accurate electronic band gaps, calculations were also carried out using the screened hybrid Heyd–Scuseria–Ernzerhof (HSE) functional.[16,17] Due to the relatively high computational cost of HSE calculations, the HSE host band gap was derived from the DOS with a Γ-centered 2×2×1 k-point mesh and Gaussian smearing of 0.025 eV.

■ RESULTS

Structure Models. In the literature, the formula of β-SiAlON:Eu^{2+} is often reported as $Si_{6-z}Al_zO_zN_{8-z}$:Eu^{2+}. However, the introduction of the Eu^{2+} activator must necessarily be charge compensated. Given that typical experimental levers to controlling synthesis involve manipulation of the nitrogen partial pressure and temperature, we have assumed that the introduction of Eu^{2+} is compensated by changes in the O/N anion ratio. Formally, we may write the chemical formula as $Si_{6-z}Al_zO_{z-2y}N_{8-z+2y}$:yEu, with *y* defining the Eu^{2+} activator concentration and *z* tuning the Si/Al ratio, or equivalently, the oxygen concentration. We will henceforth denote the exact *β*-SiAlON:Eu^{2+} composition using the abbreviation "SiAlON-*z*-*y*" throughout this work.

Figure 1b outlines the procedure used to identify Al/O/Eu ordering patterns in low-energy structures of *β*-SiAlON:Eu^{2+} in this work. In general, large supercells (≥1×1×4) are necessary to model the small Eu^{2+} activator concentrations in real phosphors. It is not computationally tractable to directly enumerate the possible orderings of Si−Al, O−N, and Eu activator for such large cells. Instead, our approach is to first identify "chemical rules" that govern the energetic preference of various species in *β*-SiAlON:Eu^{2+} based on previous experimental diffraction data and theoretical calculations.[18−21] Here, we confirmed and quantified the magnitude of these chemical preferences using a relatively small 1×1×2 supercell (four formula units) of *β*-Si_3N_4 (ICSD-34023) where three Si and one N were replaced with three Al and one O, respectively, and a single Eu^{2+} activator was introduced to maintain overall charge neutrality.

The energies of 174 symmetrically distinct $Si_9Al_3ON_{15}$:Eu^{2+} (SiAlON-1.5-0.5) were calculated. We have classified the structures into four categories based on the type of site O occupies (2*c* or 6*h* in the *β*-Si_3N_4 parent structure) and whether each O has at least one Al neighbor forming an Al−O bond. From Figure 2a, we observe that the lowest energy structure forming at least one Al−O bond is ∼1 eV lower than those without forming Al−O bond, indicating that there is a strong energetic preference for the O atom to form at least one Al−O bond. This is consistent with previous MAS NMR and theoretical observations in *β*-SiAlON.[18−20] Among these structures, we find that the structure forming an Al_3O cluster (see left structure in Figure 1b) has a significantly lower energy than other orderings (by at least 0.51 eV). Between structures having Al−O bonds (Al−O/O_{2c} and Al−O/O_{6h} in Figure 2a), the energy of the most stable structure having O in the 2*c* site is lower by 0.65 eV than the energy of the most stable structure having O in the 6*h* site. Again, this observation is in line with previous neutron diffraction observations.[21] Based on these findings, we may specify the following rules for achieving a low-energy candidate structure for *β*-SiAlON:Eu^{2+}:

1. All O must be in 2*c* sites.
2. All O must have at least one Al neighbor.

Using the above two rules, a constrained enumeration of different orderings of a 2×2×6 supercell (48 formula units, SiAlON-0.125-0.0417) was performed. The lowest energy ordering identified is given as the crystal structure on the right in Figure 1b. We may observe that the lowest energy ordering no longer has an Al_3O cluster, suggesting that the preference for an Al_3O cluster in $Si_9Al_3ON_{15}$:Eu^{2+} might be an artifact due to the small cell size. Indeed, we find that different Al orderings on the Si sublattice in the larger supercell have small energetic differences (e.g., the energy difference is less than 0.5 meV/atom for the five lowest energy structures; see Figure S1 in the Supporting Information (SI)), subject to the constraint that at least one Al is nearest neighbor to each O. This observation suggests that Al in *β*-SiAlON:Eu^{2+} may be disordered at finite temperatures.

It has been well-established that the Eu^{2+} activator sits in the large hexagonal channels in the [0001] direction.[6,7] However, the position of the Eu^{2+} activator within those channels has not been determined experimentally. Figure 2b shows the change in relative energy of the unit cell with the relative position of the Eu^{2+} activator in the [0001] direction. We find that the minimum energy position for the Eu^{2+} activator is within the same plane as the Al and O atoms. The result is that the Eu^{2+} ion is coordinated by nine nitrogens, forming a highly symmetric EuN_9 polyhedron (see Figure S2). We have also investigated other potential interstitial positions for the Eu^{2+} activator (e.g., in large hexagonal channels farther away from the O atom), but these were found to be much less energetically favorable (see Figure S3). In light of this finding, we propose an additional chemical rule to achieve a low-energy structure for *β*-SiAlON:Eu^{2+}:

3. All Al, O, and Eu must be in the same (0001) plane.

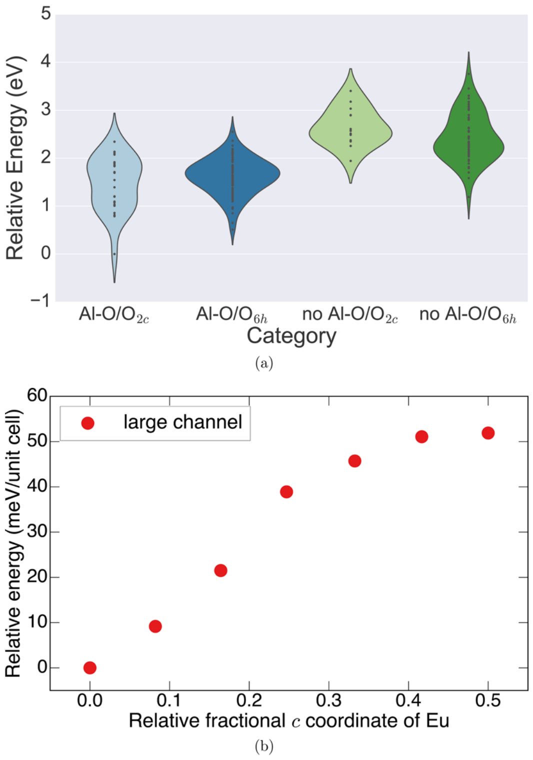

(a)

(b)

Figure 2. (a) Relative total energies of 174 symmetrically distinct structures of $Si_9Al_3ON_{15}$:Eu^{2+} (1×1×2 supercell), with the energy of the lowest energy structure set as the zero reference. The structures are divided into four categories according to whether they have at least one Al−O bond, and whether the O is in the 2*c* or 6*h* site. (b) Plot of the total energy as a function of Eu position (in fractional coordinates) with respect to the O position along [0001] direction. A relative fractional *c* coordinate of zero indicates the Eu is in the same plane as O. The energy of the most stable position is set as the zero energy reference.

These chemical rules significantly reduce the number of possible candidate structures at each composition. For subsequent investigations, we have computed the lowest energy structures for $Si_{6-z}Al_zO_{z-2y}N_{8-z+2y}$:yEu with various *z* and *y* using these chemical rules. The compositions and relaxed lattice parameters are summarized in Table 1, and the top views of ordered lowest energy structure for some of the compositions investigated are illustrated in Figure S4. Crystallographic Information Files for the final relaxed structures are also provided in the SI. The calculated lattice parameters are slightly larger (≤1%) than the reported experimental values *a* = 7.609

Table 1. Compositions, Supercell Sizes, Corresponding Values of z and y, and Relaxed Lattice Parameters a and c of $Si_{6-z}Al_zO_{z-2y}N_{8-z+2y}$:$y$Eu[a]

composition	supercell	z	y	abbreviation	a (Å)	c (Å)
Si_3N_4	1×1×1	0	0	SiAlON-0-0	7.660	2.925
$Si_{21}Al_3ON_{31}$:Eu	1×1×4	0.75	0.25	SiAlON-0.75-0.25	7.749	2.938
$Si_{69}Al_3ON_{95}$:Eu	2×2×3	0.25	0.0833	SiAlON-0.25-0.0833	7.695	2.930
$Si_{93}Al_3ON_{127}$:Eu	2×2×4	0.1875	0.0625	SiAlON-0.1875-0.0625	7.684	2.931
$Si_{117}Al_3ON_{159}$:Eu	2×2×5	0.15	0.05	SiAlON-0.15-0.05	7.681	2.928
$Si_{141}Al_3ON_{191}$:Eu	2×2×6	0.125	0.0417	SiAlON-0.125-0.0417	7.678	2.928
$Si_{140}Al_4O_2N_{190}$:Eu	2×2×6	0.167	0.0417	SiAlON-0.167-0.0417	7.676	2.929
$Si_{139}Al_5O_3N_{189}$:Eu	2×2×6	0.208	0.0417	SiAlON-0.208-0.0417	7.677	2.930
$Si_{143}AlON_{191}$	2×2×6	0.0417	0	SiAlON-0.0417-0	7.662	2.926
$Si_{141}Al_3O_3N_{189}$	2×2×6	0.125	0	SiAlON-0.125-0	7.664	2.929

[a] The lattice parameters are for the lowest energy ordering identified and normalized to the equivalent 1×1×1 hexagonal β-Si_3N_4 cell for comparison.

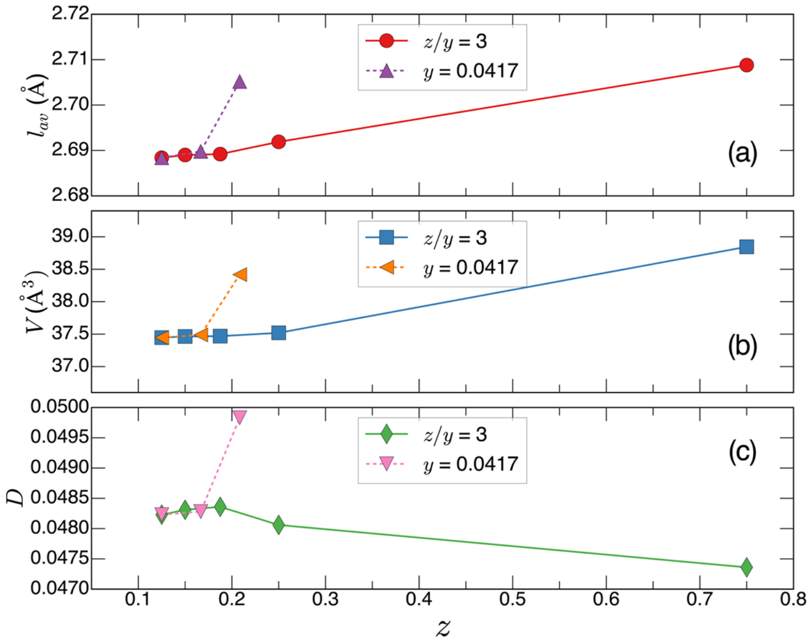

Figure 3. Calculated (a) average bond length (l_{av}), (b) polyhedron volume (V), and (c) distortion index (D) of EuN_9 polyhedron in SiAlON-z-y as a function of z for constant z/y and constant y. Lines are drawn only to guide the eyes.

Å and c = 2.9115 Å for z = 0.17 and Eu^{2+} of 0.296 mol%,[5] in line with the well-known tendency for the PBE functional to underbind.

Local Environment of Eu^{2+}. The local environment of the Eu^{2+} activator can have a critical effect on the PL properties. We have characterized the EuN_9 polyhedron local environment in β-SiAlON:Eu^{2+} using three parameters: the average bond length l_{av}, the polyhedron volume V, and the distortion index D. The distortion index is defined as

$$D = \frac{1}{n}\sum_{i=1}^{n}\frac{|l_i - l_{av}|}{l_{av}} \tag{1}$$

where l_i is the distance from the center atom to the ith coordinating atom, l_{av} is the average bond length, and n is the total number of Eu−N bonds (n = 9 in this case). A larger D implies a more distorted EuN_9 polyhedron environment.

Figure 3 shows the trends in l_{av}, V, and D for the various β-SiAlON:Eu^{2+} compositions in Table 1. We find that l_{av} ranges from 2.68 to 2.71 Å, V ranges from 37.0 to 39.0 Å^3, and D ranges from 0.0470 to 0.0500 in the compositions studied. Both l_{av} and V increase with increasing z, due to the larger Al−N (1.87 Å) and Al−O (1.75 Å) bond lengths compared to Si−N (1.74 Å).[1] At z = 0.75 in particular, the close proximity between Eu^{2+} leads to a significant volume expansion and a large l_{av} (see Figure S4a). D slightly increases and then decreases with increasing z at constant z/y. At constant y, D increases slightly with increasing in z from 0.125 to 0.167, followed by a much larger increase with further increase in z to 0.208. The reason is that the lowest energy SiAlON-0.125-0.0417 and SiAlON-0.167-0.0417 structures both have two Al neighboring the Eu^{2+} activator, while the lowest SiAlON-0.208-0.0417 has three Al neighboring the Eu^{2+} activator, resulting in a much larger distortion of the EuN_9 polyhedron.

Figure 4 shows the Eu^{2+} local environment for two representative compositions, SiAlON-0.125-0.0417 and SiAlON-0.208-0.0417. The Eu−N bonds can be classified into two types, three shorter Eu−N bonds of 2.488−2.516 Å and six longer Eu−N bonds of 2.745−2.826 Å. These results are in good agreement with the estimated bond lengths from previous EXAFS fitting (three Eu−N bonds of 2.491 Å and six Eu−N bonds of 2.891 Å) for z = 0.125 at 20 K.[7]

Photoluminescence Properties. Using the β-SiAlON:Eu^{2+} structures in Table 1, we carried out a systematic

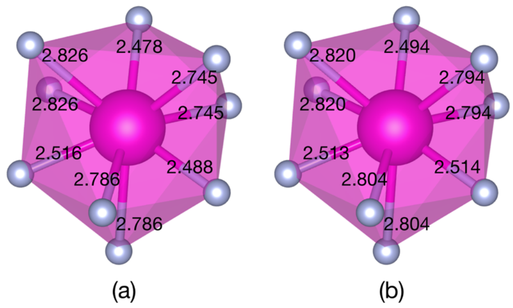

Figure 4. Symmetric EuN_9 local environment in (a) SiAlON-0.125-0.0417 and (b) SiAlON-0.208-0.0417. Maroon spheres, Eu; gray spheres N. Eu−N bond lengths are annotated in Å.

investigation of the effect of the Si/Al ratio or oxygen content (characterized by z) and concentration of the Eu^{2+} activator on the emission peak and bandwidth.

Figure 5a presents the calculated PBE ground state band structure for SiAlON-0.125-0.0417. The calculated band structures of other compositions have similar features. We may observe that the seven 4f electrons of Eu^{2+} are localized around the Fermi level, and there is a large splitting between the topmost two 4*f* levels. In a previous work, we have identified the magnitude of this splitting ΔE_S, defined as the energy gap between the topmost two 4*f* bands, as a descriptor for emission bandwidth, with narrow-band emitters having $\Delta E_S > 0.1$ eV (see inset in Figure 5a).[14] It should be noted that this splitting is based on band structures computed with the Kohn−Sham DFT approach, and therefore it does not correspond to the true $4f^7$ levels; nevertheless, the applicability of this descriptor has been tested over a variety of host structures (both broad- and narrow-band) and chemistries. The valence band maximum (VBM) of the *host* is primarily composed of N 2*p* orbital states, while the conduction band minimum (CBM) of the *host* is primarily composed of bonding states between Si 3*s*, 3*p* and N 2*p* orbitals. The Eu 4*f* and 5*d* states lie within the host band gap.

Figure 5b shows the plot of the calculated ΔE_S for z ranging from 0.125 to 0.75 with different values of y. We may observe that ΔE_S at low z concentrations are greater than 0.1 eV, implying a narrow emission bandwidth. On the other hand, ΔE_S at a large $z = 0.75$ is less than 0.1 eV, indicating a broadening in emission spectra. These predictions are in line with previous experimental observations.[1,3]

Figure 5c plots the change in the calculated HSE and PBE band gap E_g as a function of z for the undoped hosts ($y = 0$). We find that E_g decreases with increasing z, which is consistent with experimental observations.[22] We note that these results are

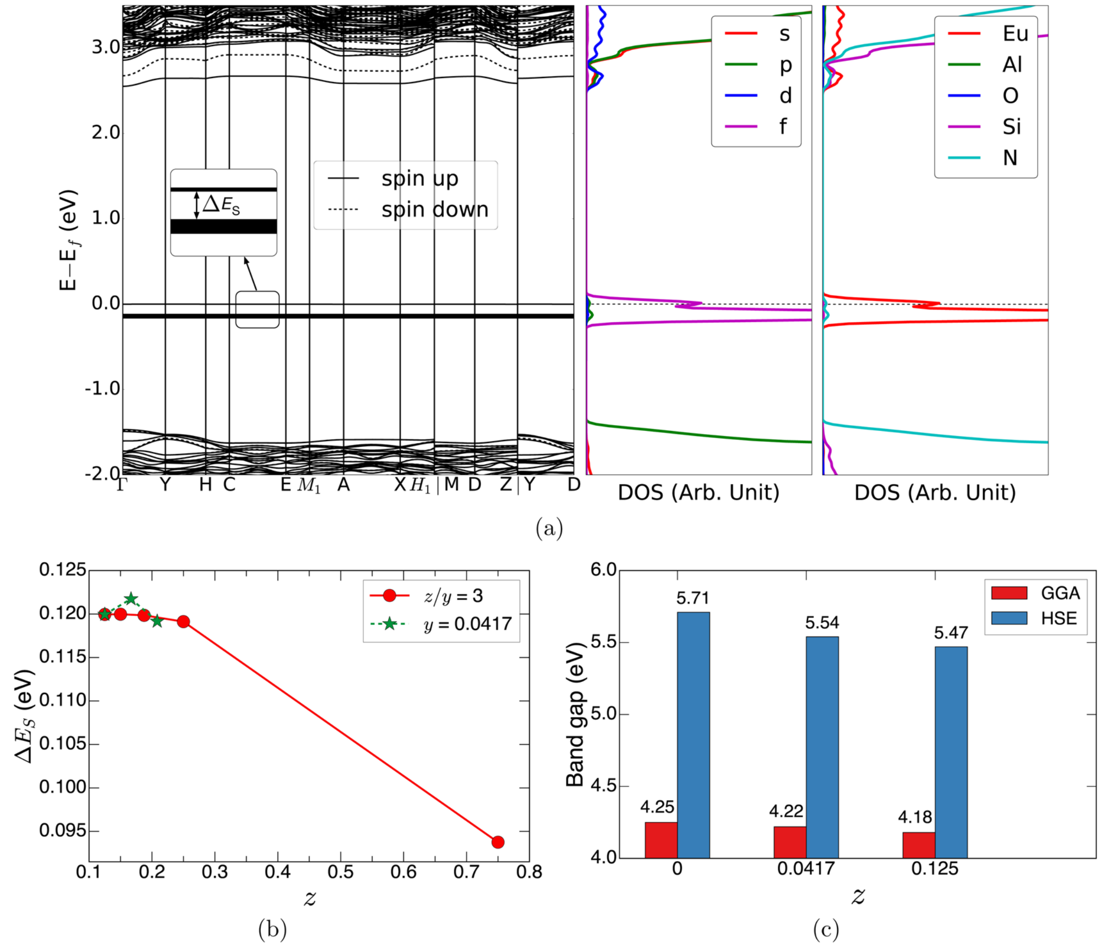

Figure 5. Calculated PL properties for SiAlON-z-y. (a) Electronic band structure and projected density of states for SiAlON-0.125−0.0417. (b) Plot of calculated bandwidth descriptor ΔE_S as a function of z. Red circles indicate compositions with the same z/y ratio. Green stars indicate compositions with the same y. The solid and dashed lines are drawn only to guide the eyes. (c) Plot of calculated undoped host ($y = 0$) band gap as a function of z.

also qualitatively consistent with previous DFT results by Tatsumi et al.,[20] though z values investigated in that work are far higher (≥ 1) than experimental compositions and the band gaps are severely underestimated due to the use of semi-local DFT functionals. The decrease of host band gap with increasing z can be ascribed to the lowering of the CBM due to increased hybridization between the N $2p$ and O $2p$ orbitals.[22] The calculated HSE E_g for β-Si_3N_4 is 5.71 eV, which is close to the G_0W_0 value of 6.06 eV[23] but somewhat lower than the experimental value (7.2 ± 0.2 eV).[22] Unsurprisingly, the semi-local PBE functional significantly underestimates the band gap.[16]

Thermal Quenching Behavior. In the auto-ionization model of Dorenbos,[24] thermal quenching occurs when a $5d$ electron in the excited state ($4f^6 5d^1$) is promoted to the conduction band of the *host* instead of relaxing back to $4f$ band. The relationship between PL emission intensity and temperature is then given by an Arrhenius relationship of the form

$$I_T = \frac{I_0}{1 + \frac{\Gamma_0}{\Gamma_\nu}\exp\left(\frac{-E_a}{k_B T}\right)} \qquad (2)$$

where I_T and I_0 are the luminescence intensity at temperature T and initial intensity at lower temperature, respectively, E_a is the energy barrier for thermal quenching, k_B is the Boltzmann's constant, Γ_0 is the attempt rate for thermal quenching at $T = \infty$, and Γ_ν is the radiative decay rate of Eu^{2+}.

Figure 6 shows the calculated *excited* band structures of SiAlON-0.125-0.0417, SiAlON-0.167-0.0417, and SiAlON-0.208-0.0417. The excited band structures of the other β-SiAlON: Eu^{2+} compositions explored in this work are given in Figure S5. It should be noted that the $4f$ bands in the excited band structures for β-SiAlON:Eu^{2+} lie below the host valence band. This is unlike previous DFT work by Jia et al.[25] on the Ce^{3+}-doped lanthanide silicate nitrides where the excited $4f$ bands lie within the band gap. However, recent work by Poncé et al.[26] on Eu^{2+}-doped barium oxynitrides similarly found that the $4f$ bands lie within the host valence band unless an atomic potential energy shift is applied. Given that we are only interested in comparisons in the relative trends in the gap between the excited $5d$ levels and the host CBM, we have not attempted to apply such a shift in this work.

From the energy gap between the excited Eu^{2+} $5d$ state and the host CBM in the *excited* band structure, we may estimate the thermal quenching activation energies E_a to be 0.56−0.68 eV. These relatively high activation energies are in reasonable agreement with the reported experimental values of 0.70−0.75 eV[2] and 0.95−1.0 eV.[1] It should be noted that direct comparison is difficult since the exact compositions obtained experimentally are not the same as those studied in this work. We also observe that E_a increases with increasing z from 0.125 to 0.167, and then decreases with increasing z from 0.167 to 0.208 at constant Eu^{2+} concentration ($y = 0.0417$).

DISCUSSION

In this section, we will present an overview of the insights that can be obtained from integrating the results reported in the previous section, with a focus on the effect of Si/Al ratio or oxygen content (z) and Eu^{2+} activator concentrations (y) on local activator environment and PL properties.

Red-Shift in Emission. Experimentally, it has been observed that the emission peak in β-SiAlON:Eu^{2+} shifts from 525 to 550 nm with increasing z from 0.1 to 2.0 at 0.7 mol % Eu^{2+}.[1] It has been speculated that the increased Stokes shift resulting from the lattice expansion was responsible for the red-shift. Our results do not support this hypothesis.

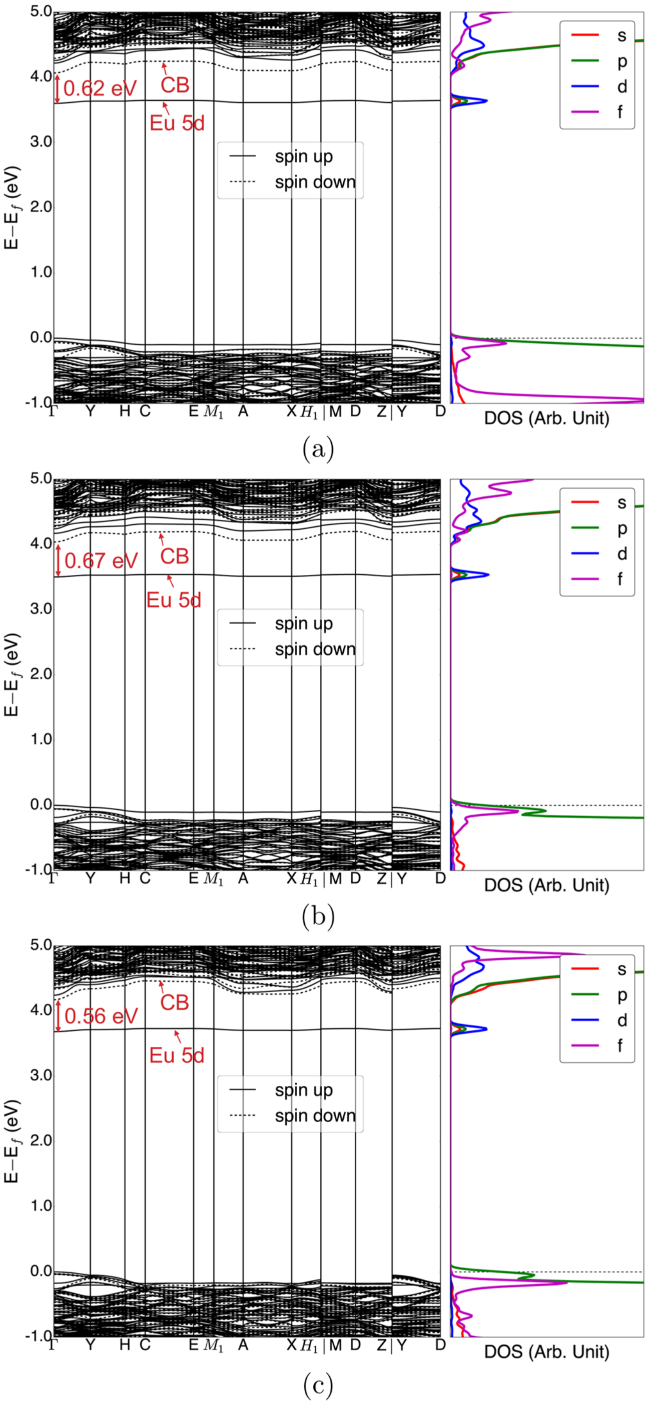

Figure 6. Calculated *excited*-state band structure and projected density of states for (a) SiAlON-0.125-0.0417, (b) SiAlON-0.167-0.0417, and (c) SiAlON-0.208-0.0417. CB denotes the host conduction band.

In general, the red-shift can be the result of a centroid shift and/or crystal field splitting in the Eu $5d$ orbitals.[27,28] Larger centroid shifts and crystal field splitting lead to longer emission wavelengths and, hence, larger red-shifts. The centroid shift is related to the nephelauxetic effect, with higher activator−anion bond covalency leading to larger centroid shifts. The magnitude of the crystal field splitting is related to the activator−anion local geometry, which can be described by the average bond length (l_{av}) and distortion index (D) of the activator−anion polyhedron. Shorter l_{av} and higher D typically lead to a larger splitting.

To assess the magnitude of the nephelauxetic effect, we have performed Bader charge analysis (see Table S1) for the EuN_9 polyhedrons in SiAlON-0.125-0.0417 and SiAlON-0.208-0.0417. We find that there are only minor changes in the effective charges on both Eu and N with increasing z, which indicate that the covalency of the Eu−N bond is not significantly affected by the nearby Al and O atoms. Based on these observations, we would argue that the nephelauxetic effect, and hence the centroid shift, is likely to play a negligible role.

From Figure 3, we find that both l_{av} and D increase with increasing z at constant y = 0.0417. However, the percentage increase in D is 3.32%, 5 times larger than the increase in l_{av} (0.63%). We speculate that the effect of increasing D dominates over the increase in l_{av}, resulting in a larger crystal field splitting with increasing z, thereby causing a red-shift in emission. We also note that the host band gap also decreases with increasing z, which may also contribute to the red-shift.

Jia et al.[25] recently adopted a ΔSCF approach combined with CDFT to estimate the absorption and emission energies, and hence, the Stokes shift. Though we were able to obtain reasonable absorption wavelengths for β-SiAlON:Eu^{2+} (331−364 nm, consistent with experimental observations[1]) using this approach, we find that emission wavelengths are significantly underestimated. It should be noted that this approach has only been tested on Ce^{3+}-doped lanthanum silicate nitrides. A more thorough assessment of this approach, especially with regard to its sensitivity to calculation parameters, choice of exchange-correlation functional, and the activator species, will be the subject of future work.

Broadening of Emission. Our results show that the oxygen concentration z has a significant effect on the descriptor for emission bandwidth ΔE_S. Large increase in z beyond 0.125 leads to ΔE_S dropping below 0.1 eV, with a corresponding broadening of the emission. This decrease in ΔE_S may be attributed to the increase in Eu−N bond length l_{av} (and EuN_9 polyhedron volume V) with increasing z (see Figure 3). As proposed in our previous work,[14] the large ΔE_S observed in narrow-band emitters (regardless of color) can be attributed to the crystal field penalty imposed by the highly symmetric EuN_9 environment. With increasing Eu−N bond lengths, this crystal field penalty is reduced, which leads to a decrease in ΔE_S. These observations provides an explanation for the previously observed broadening of the emission band with increasing oxygen content.[3] Also, oxygen content in experimental synthesis tends to be higher due to oxidation of the reactants.[3,5,7]

Thermal Quenching. From the CDFT band structures, we observe that the predicted barrier for thermal ionization in β-SiAlON:Eu^{2+} is relatively high (∼0.56−0.68 eV), which is consistent with its reported excellent thermal quenching resistance.[1,2] However, our calculations suggest that with increasing z, the thermal ionization barrier is initially increased and then reduced at constant Eu^{2+} concentration (y = 0.0417). This is somewhat contrary to Xie et al.'s experimental observations[1] that β-SiAlON's thermal stability improves monotonically with increasing z from 0.1 to 1.0 at 0.3 mol% Eu^{2+}. We are unable to explain the discrepancy, beyond noting that though a decreasing trend is seen in the DFT calculations with z ranging from 0.167 to 0.208, the barrier remains nonetheless very high (suggesting thermal stability remains good), and the range of z investigated in this work is narrower than that in the experimental study. We also note that an alternative approach to assessing thermal stability is based on the rigidity of the crystal structure, which can be estimated by calculating the Debye temperature of the host. Brgoch et al.[7] have recently performed such an analysis, where they observed that the thermal stability of β-SiAlON decreases with increasing oxygen content due to lower host structural rigidity, again at odds with the experimentally observed trend. Finally, there are many factors that can influence the measured emission intensity (e.g., synthesis condition, particle crystallinity, etc.),[29] and these factors will also affect the experimentally estimated thermal activation barrier.

Phosphor Design Insights. Composition tuning is one of the most common approaches to optimize the PL properties of phosphors. Though the effect of varying oxygen content and Eu^{2+} activator concentration on β-SiAlON has been studied extensively in the experimental literature, the main contribution of this work is establishing a direct link between composition, local Eu^{2+} activator environment, and various PL properties. To achieve narrower emission band widths and minimize red-shifting, our results suggest that synthesis should be directed toward achieving lower oxygen content in β-SiAlON. Such narrow green emitters would be highly promising for high-power LED and LCD backlighting applications. In terms of thermal stability, we would expect the effect of oxygen content to be small based on the current study as well as previous theoretical and experimental studies.[1,7]

More importantly, the general approach outlined in this work can be used in other chemical tuning efforts using first-principles calculations. For example, a topic of major interest at the present moment is in using chemical co-substitution to improve the properties of not just β-SiAlON, but also other oxide and nitride phosphors.[30,31] A similar process of elucidating the effect of such composition modifications on activator local environment using first-principles calculations can potentially yield more targeted optimization strategies to achieve a desired balance of PL properties, accelerating the phosphor design process.

CONCLUSION

In conclusion, we have performed a systematic study of structure−composition−property relationships in Eu^{2+}-activated β-SiAlON using density functional theory calculations. Using a chemical-rules-based screening approach, we identified energetically favorable models for $Si_{6-z}Al_zO_{z-2y}N_{8-z+2y}$:$y$Eu, with various Eu^{2+} activator concentrations y and Si/Al ratios (or oxygen concentrations) z. We show that the oxygen concentration z can have a significant effect on the local environment of the Eu^{2+} activator in β-SiAlON. Increasing z leads to an increase in the Eu−N bond length and increasing distortion of the EuN_9 polyhedron, which in turns leads to red-shifting and broadening of the emission. Based on these results, we suggest further reduction in oxygen content z as a pathway to achieving narrower emission band widths for high-power LED and LCD backlighting applications. Finally, the insights gained provide a constructive approach to further improvement of PL performance in not just β-SiAlON but also other phosphors.

DOI: 10.1021/acs.chemmater.6b03555
Chem. Mater. 2016, 28, 8622−8630

■ ASSOCIATED CONTENT

Supporting Information

The Supporting Information is available free of charge on the ACS Publications website at DOI: 10.1021/acs.chemmater.6b03555.

> Figures S1−S5, showing relative energies of SiAlON-0.125-0.0417, views of EuN_9 coordination polyhedron and structures, relative energies of different Eu activator sites, top views of ordered lowest energy structures, and excited-state band structures; Table S1, summarizing Bader charge analysis of EuN_9 coordination polyhedron (PDF)
>
> CIF files for nine SiAlON structures (ZIP)

■ AUTHOR INFORMATION

Corresponding Author

*E-mail: ongsp@eng.ucsd.edu.

ORCID

Zhenbin Wang: 0000-0002-7016-9245

Notes

The authors declare no competing financial interest.

■ ACKNOWLEDGMENTS

This work was supported by the National Science Foundation under Grant No. 1411192. Some of the computations in this work were performed using the Extreme Science and Engineering Discovery Environment (XSEDE), which is supported by National Science Foundation Grant No. ACI-1053575.

■ REFERENCES

(1) Xie, R.-J.; Hirosaki, N.; Li, H.-L.; Li, Y. Q.; Mitomo, M. Synthesis and Photoluminescence Properties of β-sialon: $Eu^{2+}(Si_{6-z}Al_zO_zN_{8-z}:Eu^{2+})$. *J. Electrochem. Soc.* **2007**, *154*, J314.

(2) Ho RYU, J.; Park, Y.-G.; Won, H. S.; Suzuki, H.; Kim, S. H.; Yoon, C. Luminescent properties of β-SiAlON:Eu^{2+} green phosphors synthesized by gas pressured sintering. *J. Ceram. Soc. Jpn.* **2008**, *116*, 389−394.

(3) Takahashi, K.; Xie, R.-j.; Hirosaki, N. Toward Higher Color Purity and Narrower Emission Band β-sialon:Eu^{2+} by Reducing the Oxygen Concentration. *Electrochem. Solid-State Lett.* **2011**, *14*, E38.

(4) Takeda, T.; Xie, R.-J.; Hirosaki, N. Local Structure Analysis in Nitride and Oxynitride Phosphors. *ECS J. Solid State Sci. Technol.* **2013**, *2*, R3132−R3137.

(5) Hirosaki, N.; Xie, R.-J.; Kimoto, K.; Sekiguchi, T.; Yamamoto, Y.; Suehiro, T.; Mitomo, M. Characterization and properties of green-emitting β-SiAlON:Eu^{2+} powder phosphors for white light-emitting diodes. *Appl. Phys. Lett.* **2005**, *86*, 211905.

(6) Kimoto, K.; Xie, R. J.; Matsui, Y.; Ishizuka, K.; Hirosaki, N. Direct observation of single dopant atom in light-emitting phosphor of β-SiAlON:Eu^{2+}. *Appl. Phys. Lett.* **2009**, *94*, 041908.

(7) Brgoch, J.; Gaultois, M. W.; Balasubramanian, M.; Page, K.; Hong, B. C.; Seshadri, R. Local structure and structural rigidity of the green phosphor β-SiAlON:Eu^{2+}. *Appl. Phys. Lett.* **2014**, *105*, 181904.

(8) Kresse, G.; Furthmüller, J. Efficient iterative schemes for ab initio total-energy calculations using a plane-wave basis set. *Phys. Rev. B: Condens. Matter Mater. Phys.* **1996**, *54*, 11169−11186.

(9) Blöchl, P. E. Projector augmented-wave method. *Phys. Rev. B: Condens. Matter Mater. Phys.* **1994**, *50*, 17953−17979.

(10) Ong, S. P.; Richards, W. D.; Jain, A.; Hautier, G.; Kocher, M.; Cholia, S.; Gunter, D.; Chevrier, V. L.; Persson, K. A.; Ceder, G. Python Materials Genomics (pymatgen): A robust, open-source python library for materials analysis. *Comput. Mater. Sci.* **2013**, *68*, 314−319.

(11) Perdew, J. P.; Burke, K.; Ernzerhof, M. Generalized Gradient Approximation Made Simple [Phys. Rev. Lett. 77, 3865 (1996)]. *Phys. Rev. Lett.* **1997**, *78*, 1396−1396.

(12) Dudarev, S. L.; Botton, G. A.; Savrasov, S. Y.; Humphreys, C. J.; Sutton, A. P. Electron-energy-loss spectra and the structural stability of nickel oxide: an LSDA+U study. *Phys. Rev. B: Condens. Matter Mater. Phys.* **1998**, *57*, 1505−1509.

(13) Chaudhry, A.; Boutchko, R.; Chourou, S.; Zhang, G.; Grønbech-Jensen, N.; Canning, A. First-principles study of luminescence in Eu^{2+}-doped inorganic scintillators. *Phys. Rev. B: Condens. Matter Mater. Phys.* **2014**, *89*, 155105.

(14) Wang, Z.; Chu, I.-h.; Zhou, F.; Ong, S. P. Electronic Structure Descriptor for the Discovery of Narrow-Band Red-Emitting Phosphors. *Chem. Mater.* **2016**, *28*, 4024−4031.

(15) Setyawan, W.; Curtarolo, S. High-throughput electronic band structure calculations: Challenges and tools. *Comput. Mater. Sci.* **2010**, *49*, 299−312.

(16) Heyd, J.; Scuseria, G. E.; Ernzerhof, M. Hybrid functionals based on a screened Coulomb potential. *J. Chem. Phys.* **2003**, *118*, 8207.

(17) Heyd, J.; Scuseria, G. E.; Ernzerhof, M. Erratum: Hybrid functionals based on a screened Coulomb potential [J. Chem. Phys. 118, 8207 (2003)]. *J. Chem. Phys.* **2006**, *124*, 219906.

(18) Sjöberg, J.; Harris, R. K.; Apperley, D. C. 29 Si, 27 Al and 15 N magic-angle spinning nuclear magnetic resonance study of O'-sialons and some related phases. *J. Mater. Chem.* **1992**, *2*, 433−438.

(19) Smith, M. E. Observation of mixed aluminum oxynitride $(Al(O,N)_4)$ structural units by aluminum-27 magic angle spinning NMR. *J. Phys. Chem.* **1992**, *96*, 1444−1448.

(20) Tatsumi, K.; Tanaka, I.; Adachi, H.; Yoshiya, M. Atomic structures and bondings of β- and spinel-$Si_{6-z}Al_zO_zN_{8-z}$ by first-principles calculations. *Phys. Rev. B: Condens. Matter Mater. Phys.* **2002**, *66*, 165210.

(21) Loong, C.-K.; Richardson, J. W.; Sukuzi, S.; Ozawa, M. Crystal Phase and Phonon Densities of States of β'-SiAlON Ceramics, $Si_{6-z}Al_zO_zN_{8-z}$ $(0 \leq z \leq 4)$. *J. Am. Ceram. Soc.* **1996**, *79*, 3250−3256.

(22) Boyko, T. D.; Gross, T.; Schwarz, M.; Fuess, H.; Moewes, A. The local crystal structure and electronic band gap of β-sialons. *J. Mater. Sci.* **2014**, *49*, 3242−3252.

(23) Chu, I. H.; Kozhevnikov, A.; Schulthess, T. C.; Cheng, H. P. All-electron GW quasiparticle band structures of group 14 nitride compounds. *J. Chem. Phys.* **2014**, *141*, 044709.

(24) Dorenbos, P. Thermal quenching of Eu^{2+} 5d−4f luminescence in inorganic compounds. *J. Phys.: Condens. Matter* **2005**, *17*, 8103−8111.

(25) Jia, Y.; Miglio, A.; Poncé, S.; Gonze, X.; Mikami, M. First-principles study of Ce^{3+}-doped lanthanum silicate nitride phosphors: Neutral excitation, Stokes shift, and luminescent center identification Yongchao. *Phys. Rev. B: Condens. Matter Mater. Phys.* **2016**, *93*, 155111.

(26) Poncé, S.; Jia, Y.; Giantomassi, M.; Mikami, M.; Gonze, X. Understanding Thermal Quenching of Photoluminescence in Oxynitride Phosphors from First Principles. *J. Phys. Chem. C* **2016**, *120*, 4040−4047.

(27) George, N. C.; Denault, K. A.; Seshadri, R. Phosphors for Solid-State White Lighting. *Annu. Rev. Mater. Res.* **2013**, *43*, 481−501.

(28) Li, G.; Tian, Y.; Zhao, Y.; Lin, J. Recent progress in luminescence tuning of Ce^{3+} and Eu^{2+}-activated phosphors for pc-WLEDs. *Chem. Soc. Rev.* **2015**, *44*, 8688−8713.

(29) Ha, J.; Wang, Z.; Novitskaya, E.; Hirata, G. A.; Graeve, O. A.; Ong, S. P.; McKittrick, J. An integrated first principles and experimental investigation of the relationship between structural rigidity and quantum efficiency in phosphors for solid state lighting. *J. Lumin.* **2016**, *179*, 297−305.

(30) Kurushima, T.; Gundiah, G.; Shimomura, Y.; Mikami, M.; Kijima, N.; Cheetham, A. K. Synthesis of Eu^{2+}-Activated $MYSi_4N_7$ (M = Ca,Sr,Ba) and $SrYSi_{4-x}Al_xN_{7-x}O_x$ (x = 0−1) Green Phosphors by Carbothermal Reduction and Nitridation. *J. Electrochem. Soc.* **2010**, *157*, J64.

(31) Xia, Z.; Ma, C.; Molokeev, M. S.; Liu, Q.; Rickert, K.; Poeppelmeier, K. R. Chemical Unit Cosubstitution and Tuning of

Photoluminescence in the $Ca_2(Al_{1-x}Mg_x)$ $(Al_{1-x}Si_{1+x})O_7$:Eu^{2+} Phosphor. *J. Am. Chem. Soc.* **2015**, *137*, 12494−12497.

DOI: 10.1021/acs.chemmater.6b03555